We are IntechOpen,
the world's leading publisher of
Open Access books
Built by scientists, for scientists

4,800
Open access books available

122,000
International authors and editors

135M
Downloads

154
Countries delivered to

Our authors are among the

TOP 1%
most cited scientists

12.2%
Contributors from top 500 universities

Interested in publishing with us?
Contact book.department@intechopen.com

Numbers displayed above are based on latest data collected.
For more information visit www.intechopen.com

Discrete Wavelet Analyses for Time Series

José S. Murguía and Haret C. Rosu
UASLP, IPICYT
México

1. Introduction

One frequent way of collecting experimental data by scientists and engineers is as sequences of values at regularly spaced intervals in time. These sequences are called time-series. The fundamental problem with the data in the form of time-series is how to process them in order to extract meaningful and correct information, i.e., the possible signals embedded in them. If a time-series is stationary one can think that it can have harmonic components that can be detected by means of Fourier analysis, i.e., Fourier transforms (FT). However, in recent times, it became evident that many time-series are not stationary in the sense that their mean properties change in time. The waves of infinite support that form the harmonic components are not adequate in the latter case in which one needs waves localized not only in frequency but in time as well. They have been called wavelets and allow a time-scale decomposition of a signal. Significant progress in understanding the wavelet processing of non-stationary signals has been achieved over the last two decades. However, to get the dynamics that produces a non-stationary signal it is crucial that in the corresponding time-series a correct separation of the fluctuations from the average behavior, or trend, is performed. Therefore, people had to invent novel statistical methods of detrending the data that should be combined with the wavelet analysis. A bunch of such techniques have been developed lately for the important class of non-stationary time series that display multi-scaling behavior of the multi-fractal type. Our goal in this chapter is to present our experience with the wavelet processing, based mainly on the discrete wavelet transform (DWT), of non-stationary fractal time-series of elementary cellular automata and the non-stationary chaotic time-series produced by a three-state non-linear electronic circuit.

2. The wavelet transform

Let $L^2(\mathbb{R})$ denote the space of all square integrable functions on $\mathbb{R}$. In signal processing parlance, it is the space of functions with finite energy. Let $\psi(t) \in L^2(\mathbb{R})$ be a fixed function. The function $\psi(t)$ is said to be a *wavelet* if and only if its FT $\hat{\psi}(\omega)$ satisfies

$$C_\psi = \int_0^\infty \frac{|\hat{\psi}(\omega)|^2}{|\omega|} d\omega < \infty. \tag{1}$$

The relation (1) is called the *admissibility condition* (Daubechies, 1992; Mallat, 1999; Strang, 1996; Qian, 2002), which implies that the wavelet must have a zero average

$$\int_{-\infty}^\infty \psi(t) dt = \hat{\psi}(0) = 0, \tag{2}$$

and therefore it must be oscillatory. In other words, ψ must be a sort of *wave* (Daubechies, 1992; Mallat, 1999).

Let us now define the dilated–translated wavelets $\psi_{a,b}$ as the following functions

$$\psi_{a,b}(t) = \frac{1}{\sqrt{a}}\psi\left(\frac{t-b}{a}\right), \tag{3}$$

where $b \in \mathbb{R}$ is a translation parameter, whereas $a \in \mathbb{R}^+$ ($a \neq 0$) is a dilation or scale parameter. The factor $a^{-1/2}$ is a normalization constant such that the energy, i.e., the value provided through the square integrability of $\psi_{a,b}$, is the same for all scales a. One notices that the scale parameter a in (3) rules the dilations of the independent variable $(t-b)$. In the same way, the factor $a^{-1/2}$ rules the dilation in the values taken by ψ, see the y-axis in Fig. 1. With (3), one is able to decompose a square integrable function $x(t)$ in terms of these dilated–translated wavelets.
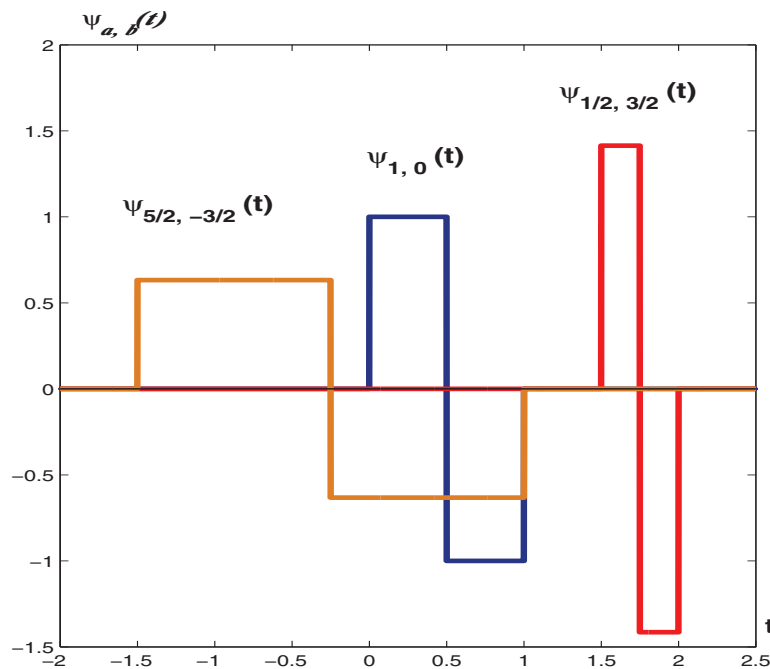

Fig. 1. The Haar wavelet function for several values of the scale parameter a and translation parameter b. If $a < 1$, the wavelet function is contracted, and if $a > 1$, the wavelet is expanded.

The *continuous wavelet transform* (CWT) of $x(t) \in L^2(\mathbb{R})$ is defined as

$$\begin{aligned} W_x(a,b) = \langle x, \psi_{a,b}\rangle &= \int_{-\infty}^{\infty} x(t)\bar{\psi}_{a,b}(t)dt \\ &= \frac{1}{\sqrt{a}}\int_{-\infty}^{\infty} x(t)\bar{\psi}\left(\frac{t-b}{a}\right)dt, \end{aligned} \tag{4}$$

where $\langle\,,\,\rangle$ is the scalar product in $L^2(\mathbb{R})$ defined as $\langle f,g\rangle := \int f(t)\bar{g}(t)dt$, and the symbol "$^-$" denotes complex conjugation. The CWT (4) measures the variation of x in a neighborhood of the point b, whose size is proportional to a.

If we are interested to reconstruct x from its wavelet transform (4), we make use of the the reconstruction formula, also called *resolution of the identity* (Daubechies, 1992; Mallat, 1999)

$$x(t) = \frac{1}{C_\psi} \int_0^\infty \int_{-\infty}^\infty W_x(a, b) \psi_{a,b}(t) \frac{dadb}{a^2}, \tag{5}$$

where it is now clear why we imposed (1).

However, a huge amount of data are represented by a finite number of values, so it is important to consider a discrete version of the CWT (4). Generally, the orthogonal(discrete) wavelets are employed because this method associates the wavelets to orthonormal bases of $L^2(\mathbb{R})$. In this case, the wavelet transform is performed only on a discrete grid of the parameters of dilation and translation, i.e., a and b take only integral values. Within this framework, an arbitrary signal $x(t)$ of finite energy can be written using an orthonormal wavelet basis:

$$x(t) = \sum_m \sum_n d_n^m \psi_n^m(t), \tag{6}$$

where the coefficients of the expansion are given by

$$d_n^m = \int_{-\infty}^\infty x(t) \psi_n^m(t) dt . \tag{7}$$

The orthonormal basis functions are all *dilations* and *translations* of a function referred as the analyzing wavelet $\psi(t)$, and they can be expressed in the form

$$\psi_n^m(t) = 2^{m/2} \psi(2^m t - n), \tag{8}$$

with m and n denoting the dilation and translation indices, respectively. The contribution of the signal at a particular wavelet level m is given by

$$d_m(t) = \sum_n d_n^m \psi_n^m(t), \tag{9}$$

which provides information on the time behavior of the signal within different scale bands. Additionally, it provides knowledge of their contribution to the total signal energy.

In this context, Mallat (1999) developed a computationally efficient method to calculate (6) and (7). This method is known as multiresolution analysis (MRA). The MRA approach provides a general method for constructing orthogonal wavelet basis and leads to the implementation of the fast wavelet transform (FWT). This algorithm connects, in an elegant way, wavelets and filter banks. A multiresolution signal decomposition of a signal X is based on successive decomposition into a series of approximations and details, which become increasingly coarse. Associated with the wavelet function $\psi(t)$ is a corresponding scaling function, $\varphi(t)$, and scaling coefficients, a_n^m (Mallat, 1999). The scaling and wavelet coefficients at scale m can be computed from the scaling coefficients at the next finer scale $m + 1$ using

$$a_n^m = \sum_l h[l - 2n] a_l^{m+1}, \tag{10}$$

$$d_n^m = \sum_l g[l - 2n] a_l^{m+1}, \tag{11}$$

where $h[n]$ and $g[n]$ are typically called lowpass and highpass filters in the associated filter bank. Equations (10) and (11) represent the fast wavelet transform (FWT) for computing (7). In

fact, the signals a_n^m and d_n^m are the convolutions of a_n^{m+1} with the filters $h[n]$ and $g[n]$ followed by a downsampling of factor 2 (Mallat, 1999).

Conversely, a reconstruction of the original scaling coefficients a_n^{m+1} can be made from

$$a_n^{m+1} = \sum_l \left(h[2l-n]a_l^m + g[2l-n]d_l^m \right), \tag{12}$$

a combination of the scaling and wavelet coefficients at a coarse scale. Equation (12) represents the inverse of FWT for computing (6), and it corresponds to the synthesis filter bank. This part can be viewed as the discrete convolutions between the upsampled signal a_l^m and the filters $h[n]$ and $g[n]$, that is, following an "upsampling" of factor 2 one calculates the convolutions between the upsampled signal and the filters $h[n]$ and $g[n]$. The number of levels in the multiresolution algorithm depends on the length of the signal. A signal with 2^k values can be decomposed into $k+1$ levels. To initialize the FWT, one considers a discrete time signal $X = \{x[1], x[2], \ldots, x[N]\}$ of length $N = 2^M$. The first application of (10) and (11), beginning with $a_n^{m+1} = x[n]$, defines the first level of the FWT of X. The process goes on, always adopting the "$m+1$" scaling coefficients to calculate the "m" scaling and wavelet coefficients. Iterating (10) and (11) M times, the transformed signal consists of M sets of wavelet coefficients at scales $m = 1, \ldots, M$, and a signal set of scaling coefficients at scale M. There are exactly $2^{(k-m)}$ wavelet coefficients d_n^m at each scale m, and $2^{(k-M)}$ scaling coefficients a_n^M. The maximum number of iterations $M_{\max}$ is k. This property of the MRA is generally the key factor to identify crucial information in the respective frequency bands. A three-level decomposition process of the FWT is shown in Fig. 2.
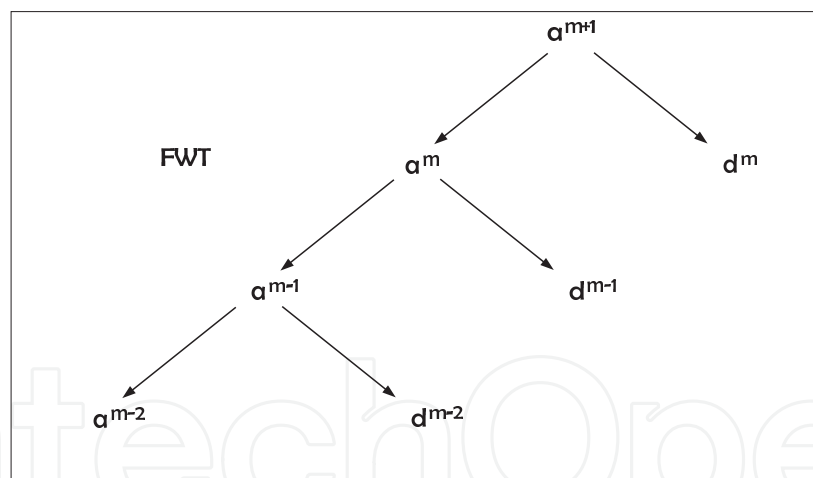

Fig. 2. The structure of a three-level fast wavelet transform.

In a broad sense, with this approach, the low-pass coefficients capture the trend and the high-pass coefficients keep track of the fluctuations in the data. The scaling and wavelet functions are naturally endowed with an appropriate window size, which manifests in the scale index or level, and hence they can capture the local averages and differences, in a window of one's choice.

When someone is interested to measure the local or global regularity of a signal, some degree of regularity is useful in the wavelet basis for the representation to be well behaved (Daubechies, 1992; Mallat, 1999). To achieve this, a wavelet function should have n vanishing moments. A wavelet is said to have n vanishing moments if and only if it satisfies $\int_{-\infty}^{\infty} t^k \psi(t)dt = 0$ for $k = 0, 1, \ldots, n-1$ and $\int_{-\infty}^{\infty} t^k \psi(t)dt \neq 0$ for $k = n$. This means that

a wavelet with n vanishing moments is orthogonal to all polynomials up to order $n-1$. Thus, the DWT of $x(t)$ performed with a wavelet $\psi(t)$ with n vanishing moments is nothing else but a "smoothed version" of the $n-$th derivative of $x(t)$ on various scales. This important property helps detrending the data.

In addition, another important property is that the total energy of the signal may be expressed as follows

$$\sum_{n=1}^{N}|x[n]|^2 = \sum_{n=1}^{N}|a_n^M|^2 + \sum_{m=1}^{M}\sum_{n=1}^{N}|d_n^m|^2. \tag{13}$$

This can be identified as Parseval's relation in terms of wavelets, where the signal energy can be calculated in terms of the different resolution levels of the corresponding wavelet-transformed signal. A more detailed treatment of this subject can be found in (Mallat, 1999).

3. Multifractal analysis of cellular automata time series

3.1 Cellular automata

An elementary cellular automaton(ECA) can be considered as a discrete dynamical that evolve at discrete time steps. An ECA is a cellular automata consisting of a chain of N lattice sites with each site is denoted by an index i. Associated with each site i is a dynamical variable x_i which can take only k discrete values. Most of the studies have been done with $k = 2$, where $x_i = 0$ or 1. Therefore there are 2^N different states for these automata. One can see that the time, space, and states of this system take only discrete values. The ECA considered evolves according to the local rule

$$x_n^{t+1} = [x_{n-1}^t + x_{n+1}^t]\mathrm{mod}\,2\,, \tag{14}$$

which corresponds to the rule 90. Table 1 is the lookup table of this ECA rule, where it is specified the evolution from the neighborhood configuration (first row) to the next state (second row), that is, the next state of $i-$th cell depends on the present states of its left and right neighbors.

Neighborhood	111	110	101	100	011	010	001	000
Rule result	0	1	0	1	1	0	1	0

Table 1. Elementary rule 90. The second row shows the future state of the cell if it and its neighbors are in the arrangement shown above in the first row.

In fact, a rule is numbered by the unsigned decimal equivalent of the binary expression in the second row. When the same rule is applied to update cells of ECA, such ECA are called uniform ECA; otherwise the ECA are called non-uniform or hybrids. It is important to observe that the evolution rules of ECA are determined by two main factors, the rule and the initial conditions.

3.2 WMF-DFA algorithm

To reveal the MF properties (Halsey et al., 1986) of ECA, we follow a variant of the MF-DFA with the discrete wavelet method proposed in (Manimaran et al., 2005). This algorithm will separate the trends from fluctuations, in the ECA time series, using the fact that the low-pass version resembles the original data in an "averaged" manner in different resolutions. Instead

of a polynomial fit, we consider the different versions of the low-pass coefficients to calculate the "local" trend. This method involves the following steps.

Let $x(t_k)$ be a time series type of data, where $t_k = k\Delta t$ and $k = 1, 2, \ldots, N$.

1. Determine the profile $Y(k) = \sum_{i=1}^{k}(x(t_i) - \langle x \rangle)$ of the time series, which is the cumulative sum of the series from which the series mean value is subtracted.

2. Compute the fast wavelet transform (FWT), i.e., the multilevel wavelet decomposition of the profile. For each level m, we get the fluctuations of the $Y(k)$ by subtracting the "local" trend of the Y data, i.e., $\Delta Y(k; m) = Y(k) - \tilde{Y}(k; m)$, where $\tilde{Y}(k; m)$ is the reconstructed profile after removal of successive details coefficients at each level m. These fluctuations at level m are subdivided into windows, i.e., into $M_s = \text{int}(N/s)$ non-overlapping segments of length s. This division is performed starting from both the beginning and the end of the fluctuations series (i.e., one has $2M_s$ segments). Next, one calculates the local variances associated to each window ν

$$F^2(\nu, s; m) = \text{var}\left[\Delta Y((\nu - 1)s + j; m)\right] , j = 1, ..., s , \nu = 1, ..., 2M_s , M_s = \text{int}(N/s) . \quad (15)$$

3. Calculate a $q-$th order fluctuation function defined as

$$F_q(s; m) = \left\{ \frac{1}{2M_s} \sum_{\nu=1}^{2M_s} |F^2(\nu, s; m)|^{q/2} \right\}^{1/q} \quad (16)$$

where $q \in \mathbb{Z}$ with $q \neq 0$. Because of the diverging exponent when $q \rightarrow 0$ we employed in this limit a logarithmic averaging $F_0(s; m) = \exp\left\{ \frac{1}{2M_s} \sum_{\nu=1}^{2M_s} \ln |F^2(\nu, s; m)| \right\}$ as in (Kantelhardt et al., 2002; Telesca et al., 2004).

To determine if the analyzed time series have a fractal scaling behavior, the fluctuation function $F_q(s; m)$ should reveal a power law scaling

$$F_q(s; m) \sim s^{h(q)}, \quad (17)$$

where $h(q)$ is called the generalized Hurst exponent (Telesca et al., 2004) since it can depend on q, while the original Hurst exponent is $h(2)$. If h is constant for all q then the time series is monofractal, otherwise it has a MF behavior. In the latter case, one can calculate various other MF scaling exponents, such as $\tau(q) = qh(q) - 1$ and $f(\alpha)$ (Halsey et al., 1986). A linear behavior of $\tau(q)$ indicates monofractality whereas the non-linear behavior indicates a multifractal signal. A fundamental result in the multifractal formalism states that the singularity spectrum $f(\alpha)$ is the Legendre transform of $\tau(q)$, i.e.,

$$\alpha = \tau'(q), \qquad \text{and} \qquad f(\alpha) = q\alpha - \tau(q).$$

The singularity spectrum $f(\alpha)$ is a non-negative convex function that is supported on the closed interval $[\alpha_{\min}, \alpha_{\max}]$. In fact, the strength of the multifractality is roughly measured with the width $\Delta\alpha = \alpha_{\max} - \alpha_{\min}$ of the parabolic singularity spectrum $f(\alpha)$ on the α axis, where the boundary values of the support, $\alpha_{\min}$ for $q > 0$ and $\alpha_{\max}$ for $q < 0$, correspond to the strongest and weakest singularity, respectively.

3.3 Application of WMF-DFA

To illustrate the efficiency of the wavelet multifractal procedure, we first carry out the analysis of the binomial multifractal model (Feder, 1998; Kantelhardt et al., 2002).

For the multifractal time series generated through the binomial multifractal model , a series of $N = 2^{n_{max}}$ numbers x_k, with $k = 1, \ldots, N$, is defined by

$$x_k = a^{n(k-1)}(1-a)^{n_{max}-n(k-1)}. \tag{18}$$

where $0.5 < a < 1$ is a parameter and $n(k)$ is the number of digits equal to 1 in the binary representation of the index k. The scaling exponent $h(q)$ and $\tau(q)$ can be calculated exactly in this model. These exponents have the closed form

$$h(q) = \frac{1}{q} - \frac{\ln[a^q + (1-a)^q]}{q \ln 2}, \qquad \tau(q) = -\frac{\ln[a^q + (1-a)^q]}{\ln 2}. \tag{19}$$

In Table 2 and Fig. 3, we present the comparison of the multifractal quantity h for $a = 2/3$ between the values for the theoretical case ($h_T(q)$), with the numerical results obtained through wavelet analysis ($h_W(q)$). Notice that the numerical values have a slight downward translation. Adding a vertical offset ($\Delta = h_T(1) - h_W(1)$) to $h_W(q)$, we can notice that both values theoretically and numerically are very close.

q	$h_T(q)$	$h_W(q)$	$h_W(q) + \Delta$
-10	1.4851	1.4601	1.4851
-9	1.4742	1.4498	1.4749
-8	1.4607	1.4373	1.4623
-7	1.4437	1.4217	1.4467
-6	1.4220	1.4018	1.4269
-5	1.3938	1.3761	1.4012
-4	1.3568	1.3422	1.3673
-3	1.3083	1.2971	1.3221
-2	1.2459	1.2376	1.2627
-1	1.1699	1.1626	1.1876
0	0.0000	1.0742	1.0992
1	1.0000	0.9809	1.0059
2	0.9240	0.8961	0.9212
3	0.8617	0.8286	0.8537
4	0.8131	0.7780	0.8031
5	0.7761	0.7401	0.7652
6	0.7479	0.7112	0.7362
7	0.7262	0.6887	0.7137
8	0.7093	0.6711	0.6961
9	0.6958	0.6570	0.6821
10	0.6848	0.6457	0.6707

Table 2. The values of the generalized Hurst exponent h for the binomial multifractal model with $a = 2/3$, which were computed analytically and with the wavelet approach.

In a similar way, we analyze the time series of the so-called row sum ECA signals, i.e., the sum of ones in sequences of rows, employing the db-4 wavelet function, another wavelet function that belongs to the Daubechies family (Daubechies, 1992; Mallat, 1999). We have found that
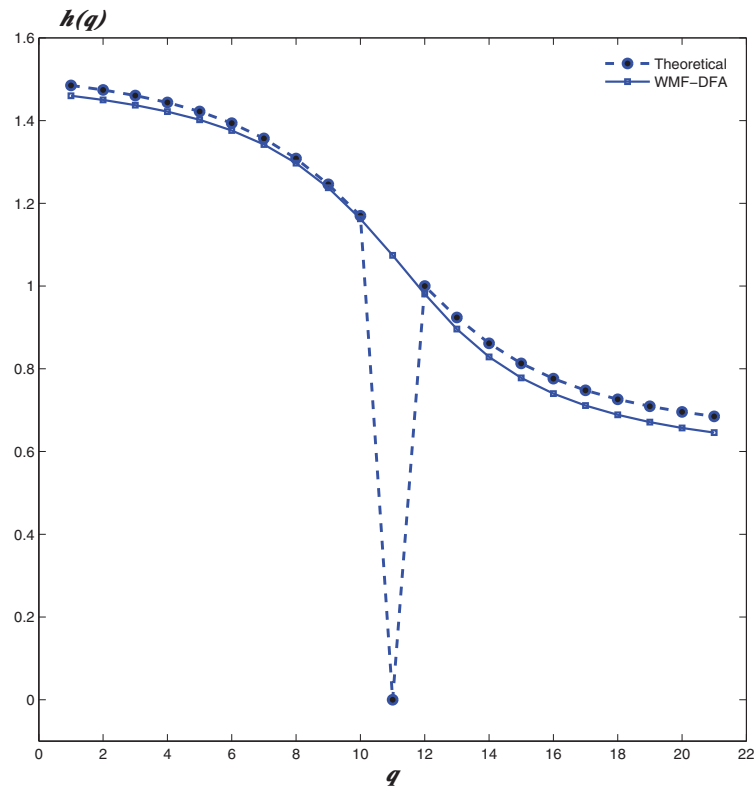
Fig. 3. The generalized Hurst exponent h for the binomial multifractal model with $a = 2/3$. The theoretical values of $h(q)$ with the WMF-DFA calculations are shown for comparison.

a better matching of the results given by the WMF-DFA method with those of other methods is provided with this wavelet function. Figure 4 illustrates the results for the rule 90, when the first row is all 0s with a 1 in the center, i.e., the impulsive initial condition. The fact that the generalized Hurst exponent is not a constant horizontal line is indicative of a multifractal behavior in this ECA time series. In addition, if the τ index is not of a single slope, it can be considered as another clear feature of multifractality.

For the impulsive initial condition in ECA rule 90 the most "frequent" singularity for the analyzed time series occurs at $\alpha = 0.568$, and $\Delta\alpha = 1.0132(0.9998)$ when the WMF-DFA (MF-DFA) are employed. Reference (Murguía et al., 2009) presents the results for different initial center pulses for rules 90, 105, and 150, where the width $\Delta\alpha$ of rule 90 is shifted to the right with respect to those of 105 and 150. In addition, the strongest singularity, $\alpha_{\min}$, of all these time series corresponds to the rule 90 and the weakest singularity, $\alpha_{\max}$, to the rule 150. With the aim of computing the pseudo-random sequences of N bits, in Reference (Mejía & Urías, 2001) an algorithm based on the backward evolution of the CA rule 90 has been proposed. A modification of the generator producing pseudo-random sequences has been recently considered in (Murguía et al., 2010). The latter proposal is implemented and studied in terms of the sequence matrix $\mathbf{H}_N$, which was used to generate recursively the pseudo-random sequences.

This matrix has dimensions $(2N + 1) \times (2N + 1)$. Since the evolution of the sequence matrix $\mathbf{H}_N$ is based on the evolution of the ECA rule 90, the structure of the patterns of bits of the latter must be directly reflected in the structure of the entries of $\mathbf{H}_N$.
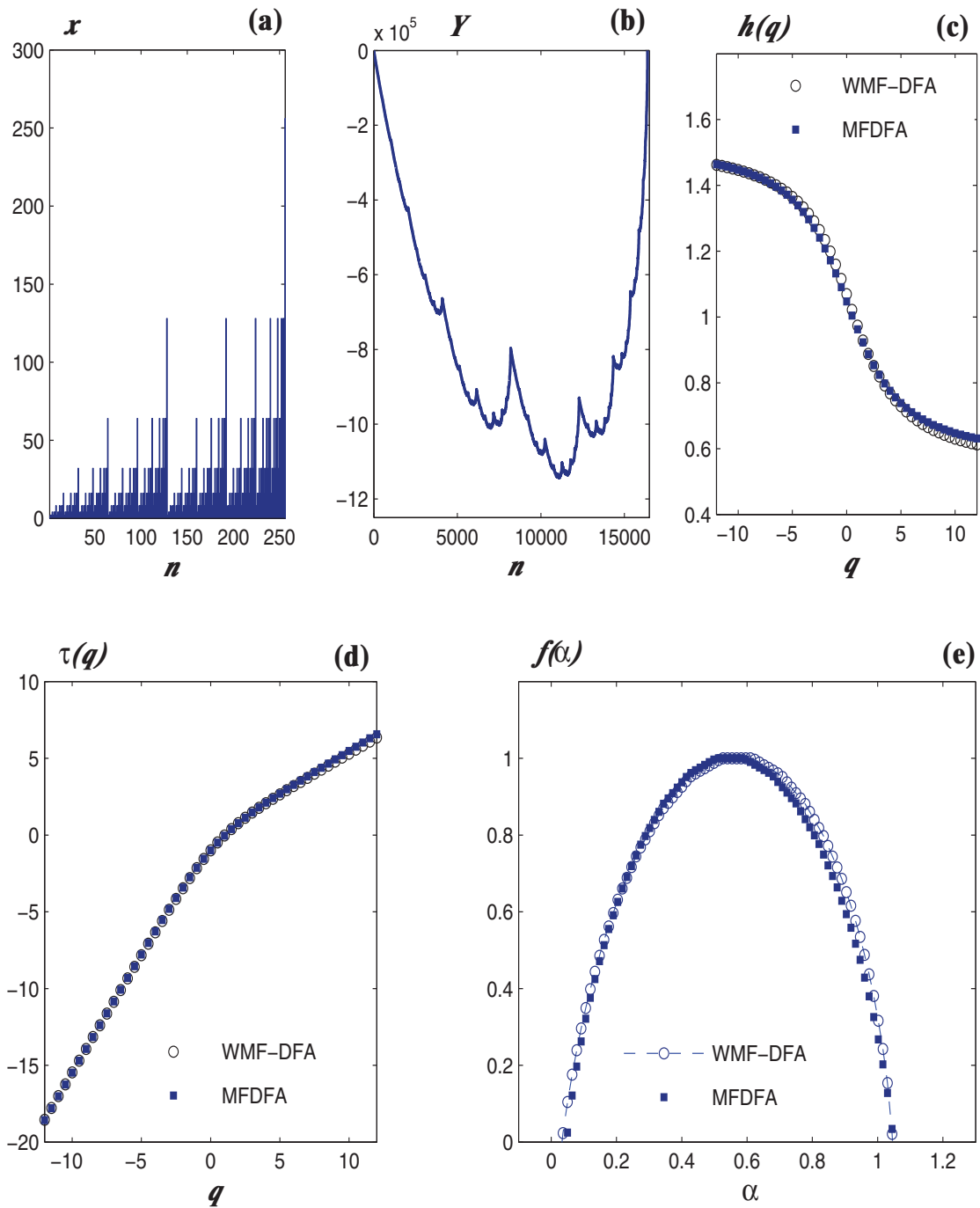
Fig. 4. (a) Time series of the row signal of the cellular automata rule 90. Only the first 2^8 points are shown of the whole set of 2^{14} data points. Profile Y of the row signal. (d) Generalized Hurst exponent $h(q)$. (e) The τ exponent, $\tau(q) = qh(q) - 1$. (f) The singularity spectrum $f(\alpha) = q\frac{d\tau(q)}{dq} - \tau(q)$. The calculations of the multifractal quantities h, τ, and $f(\alpha)$ are performed both with the MF-DFA and the wavelet-based WMF-DFA.

Here, in the same spirit as in Ref. (Murguía et al., 2009), we also analyze the sum of ones in the sequences of the rows of the matrix $\mathbf{H}_N$ with the db-4 wavelet function. The results for the row sums of $\mathbf{H}_{2047}$ are illustrated in Fig. 5, through which we confirm the multifractality of this time series. The width $\Delta \alpha_{H_{2047}} = 1.12 - 0.145 = 0.975$, and the most "frequent" singularity occurs at $\alpha_{\mathrm{mf}_{H_{2047}}} = 0.638$. Although the profile is different, the results are similar with those obtained for the rule 90 with a slight shifting, see Fig. 4. A more complete analysis of this matrix is carried out in (Murguía et al., 2010).

4. Chaotic time series

In this section, we study the dynamics of experimental time series generated by an electronic chaotic circuit. The wavelet analysis of these experimental chaotic time series gives us useful information of such system through the energy concentration at specific wavelet levels.

It is known that the wavelet variance provides a very efficient measure of the structure contained within a time series because of the ability of wavelet transforms to allot small wavelet coefficients to the smoother parts of a signal in contrast with the sharp, non-stationary behavior which gives rise to local maxima (see, for example, Chapter 8 in the book of Percival and Walden (Percival & Walden, 2000)).

4.1 Chaotic electronic circuit

The electronic circuit of Fig. 6 (a) has been employed to study chaos synchronization (Rulkov, 1996; Rulkov & Sushchik, 1997). This circuit, despite its simplicity, exhibits complex chaotic dynamics and it has received wide coverage in different areas of mathematics, physics, engineering and others (Campos-Cantón et al., 2008; Rulkov, 1996; Rulkov & Sushchik, 1997). It consists of a linear feedback and a nonlinear converter, which is the block labeled N. The linear feedback is composed of a low-pass filter RC' and a resonator circuit rLC.

The dynamics of this chaotic circuit is very well modeled by the following set of differential equations:

$$\begin{aligned}
\dot{x} &= y, \\
\dot{y} &= z - x - \delta y, \\
\dot{z} &= \gamma \left[k f(x) - z \right] - \sigma y,
\end{aligned} \tag{20}$$

where $x(t)$ and $z(t)$ are the voltages across the capacitors, C and C', respectively, and $y(t) = J(t)(L/C)^{1/2}$ is the current through the inductor L. The unit of time is given by $\tau = 1/\sqrt{LC}$. The parameters γ, δ, and σ have the following dependence on the physical values of the circuit elements: $\gamma = \sqrt{LC}/RC'$, $\delta = r\sqrt{C/L}$ and $\sigma = C/C'$. The main characteristic of the nonlinear converter N in Fig. 6 is to transform the input voltage $x(t)$ into an output voltage with nonlinear dependence $F(x) = k f(x)$ on the input. The parameter k corresponds to the gain of the converter at $x = 0$. The detailed circuit structure of N is shown in Fig. 6 (b).

It is worth mentioning that depending on the component values of the linear feedback and the parameter k, the behavior of the chaotic circuit can be in regimes of either *periodic* or *chaotic* oscillations. Due to the characteristics of the inductor in the linear feedback, it turns out to be hard to scale to arbitrary frequencies and analyze it because of its frequency-dependent resistive losses. Therefore, the parameter k has been considered to analyze this chaotic circuit, since it appeared to be a very useful bifurcation parameter in both the numerical and experimental cases (Campos-Cantón et al., 2008). Two different attractors, projected on the plane (x, y), generated by this electronic circuit, are shown in Fig. 7. These attractors have
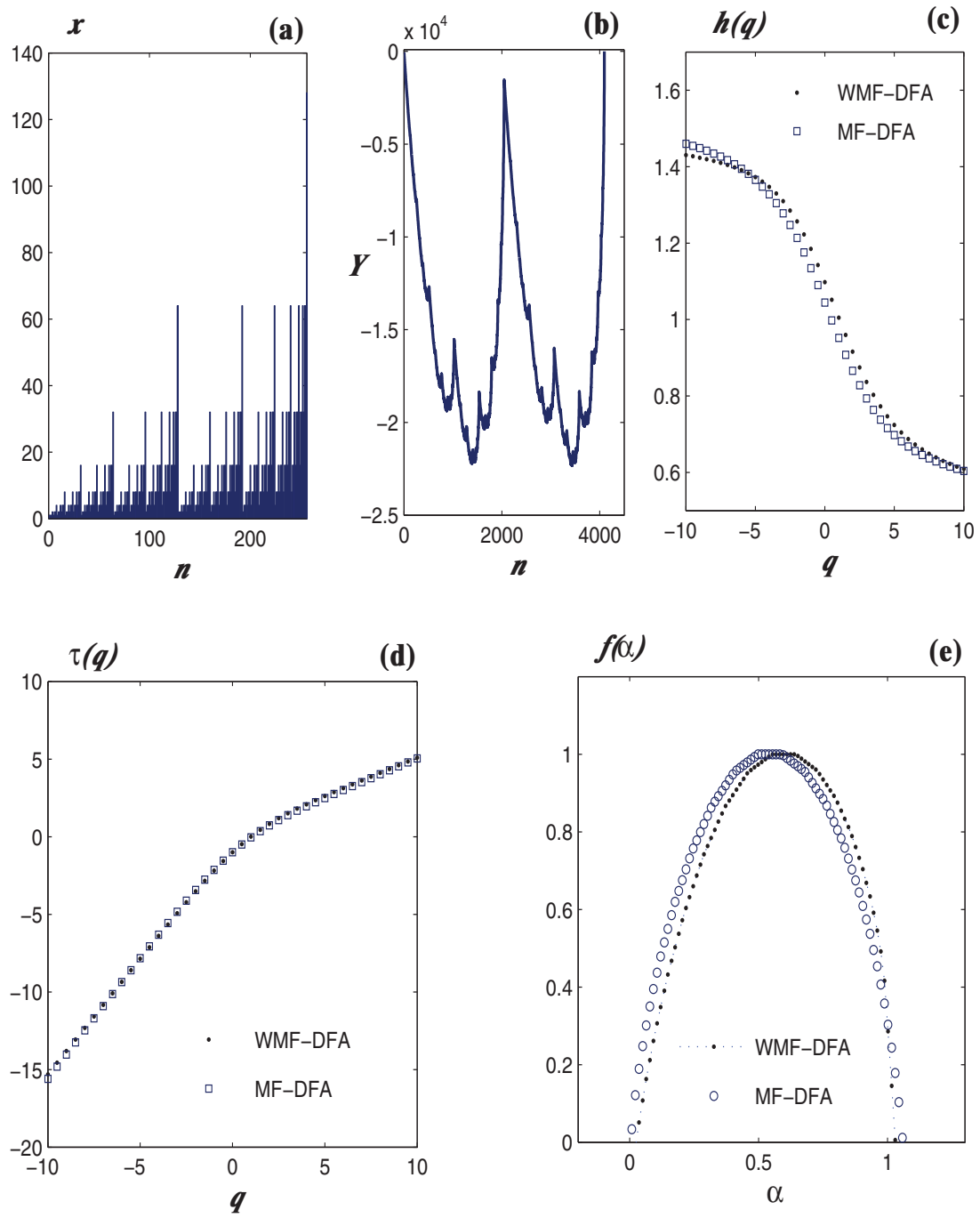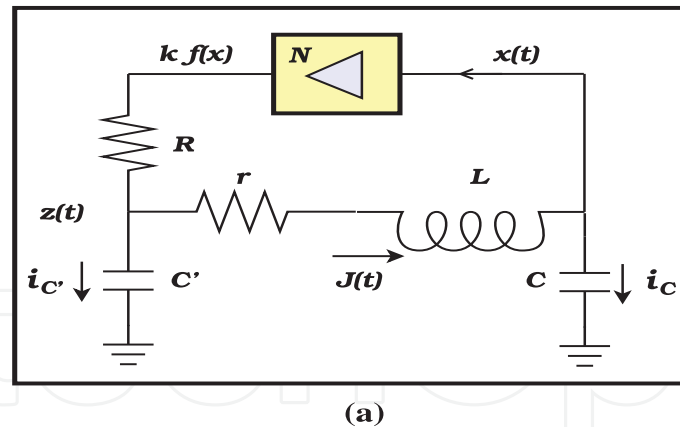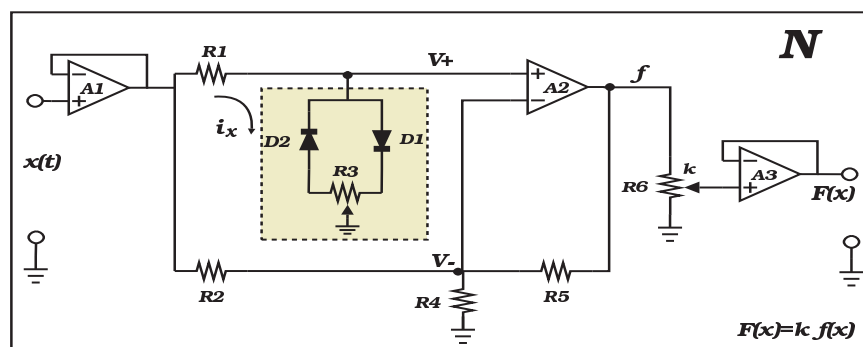
Fig. 5. (a) Time series of the row signal of $\mathbf{H}_{2047}$. Only the first 256 points are shown of the whole set of $2^{11} - 1$ data points. (b) Profile of the row signal of $\mathbf{H}_{2047}$. (c) Generalized Hurst exponent $h(q)$, (d) the $\tau(q)$ exponent, and (e) the singularity spectrum $f(\alpha)$.

(a)

(b)

Fig. 6. (a) The circuit diagram of a nonlinear chaotic oscillator. The component values employed are $C' = 100.2$ nF, $C = 200.1$ nF, $L = 63.8$ mH, $r = 138.9$ Ω, and $R = 1018$ Ω. (b) Schematic diagram of the nonlinear converter N. The electronic component values are $R1 = 2.7$ kΩ, $R2 = R4 = 7.5$ kΩ, $R3 = 50$ Ω, $R5 = 177$ kΩ, $R6 = 20$ kΩ. The diodes D1 and D2 are 1N4148, the operational amplifiers A1 and A2 are both TL082, and the operational amplifier A3 is LF356N.

a shape similar to a Rössler oscillator (Fig. 7(a)), and to a double scroll oscillator (Fig. 7(b)). They can be easily obtained by just fixing the bifurcation parameter k to be equal to 0.4010, and 0.3964, respectively.

4.2 Wavelet variance

In the wavelet approach the fractal character of a certain signal can be inferred from the behavior of its power spectrum $P(\omega)$, which is the Fourier transform of the autocorrelation function and in differential form $P(\omega)d\omega$ represents the contribution to the variance of the part of the signal contained between frequencies ω and $\omega + d\omega$. Indeed, it is known that for self-similar random processes the spectral behavior of the power spectrum is given by

$$P(\omega) \sim | \omega |^{-\beta}, \tag{21}$$

where β is the spectral parameter of the signal. In addition, the variance of the wavelet coefficients var $\{d_n^m\}$ is related to the level m through a power law of the type (Wornell & Oppenheim, 1992)
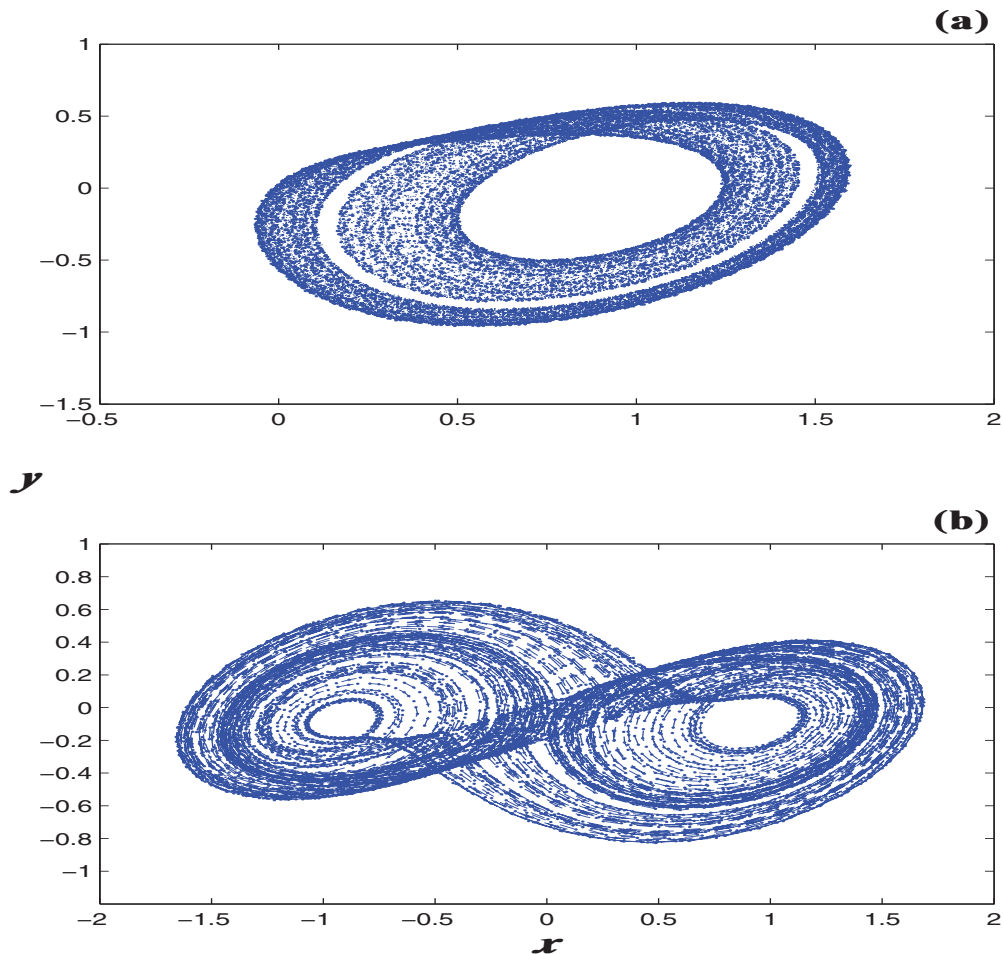
Fig. 7. Attractors of the electronic chaotic circuit projected on the plane $x - y$ obtained experimentally for two different values of the bifurcation parameter k: (a) 0.4010, and (b) 0.3964.

$$\text{var}\,\{d_n^m\} \approx (2^m)^{-\beta}. \tag{22}$$

This wavelet variance has been used to find dominant levels associated with the signal, for example, in the study of numerical and experimental chaotic time series (Campos-Cantón et al., 2008; Murguía & Campos-Cantón, 2006; Staszewski & Worden, 1999). In order to estimate β we used a least squares fit of the linear model

$$\log_2(\text{var}\{d_n^m\}) = \beta_m + (K + v_m), \tag{23}$$

where K and v_m are constants related to the linear fitting procedure. Equation (22) is certainly suitable for studying discrete chaotic time series, because their variance plot has a well-defined form as pointed out in (Murguía & Campos-Cantón, 2006; Staszewski & Worden, 1999). If the variance plot shows a maximum at a particular scale, or a bump over a group of scales, which means a high energy concentration, it will often correspond to a coherent

structure. In general, the gradient of a noisy time series turns out to be zero in the variance plot, therefore it does not show any energy concentration at specific wavelet level. In certain cases the gradient of some chaotic time series has a similar appearance with Gaussian noise at lower scales, which implies that these chaotic time series do not present a fundamental "carrier" frequency at any scale.

For our illustrative analysis and comparison with the experiments, we study the time series of the x states of the attractors displayed in Fig. 7(a)-(b), because they are of very different type and we want to emphasize the versatility of the wavelet approach. The acquisition of the experimental data was carried out with a DAQ with a sampling frequency of 180 kHz, i.e. we collected the experimental data for a total time of 182 ms for both signals. In the analysis of these time series we employed the db-8 wavelet, a wavelet function that belongs to the Daubechies family (Daubechies, 1992; Mallat, 1999).

- Case $k = 0.4010$.

  The first time series to consider corresponds to the x state of the experimental attractor of Fig. 7 (a). The first 12 ms of this time series are shown in Fig. 8 (a), whereas Fig. 8 (b) shows a semi-logarithmic plot of the wavelet coefficient variance as a function of level m, which is denominated as variance plot of the wavelet coefficients. One can notice that the whole series is dominated by the 12th wavelet level, i.e., this wavelet level has the major energy concentration, and it is plotted in isolation in Fig. 8 (c). The energy rate between the reconstructed signal with respect to the original signal was $(E_{x_{12}}/E_x) = 0.9565$, which means an energy close to 96% of the total one in this case. Since it does not properly show the structure of the chaotic time series, we considered and added together the three neighbor wavelet levels, $m = 11 - 13$, achieving an energy concentration of 99% of the total one. In this case, the reconstruction of the signal at these wavelet levels is shown in Fig. 8(d), where the structure of the original signal can be noticed. Both reconstructed time series present a slight downward translation, because of the DC component of this chaotic time series.

- Case $k = 0.3964$.

  For this value of k, the behaviour of the chaotic electronic circuit is similar to that of a double scroll oscillator with the shape of the attractor displayed in Fig. 7. The experimental time series corresponding to the x state of this attractor is shown in Fig. 9 (a), while the variance plot is given in Fig. 9 (b) where the gradient is close to zero, which means that no significant energy concentration can be seen. We have found that when summing over the wavelet levels $m = 6 - 12$ the energy concentration is close to 99% of the total one but without any pronounced peak. Thus, this case does not present a fundamental "carrier" frequency and therefore this attractor has a Gaussian noisy behavior. The reconstructed time series with the mentioned wavelet levels is displayed in Fig. 9 (c).

5. Conclusion

The DWT is currently a standard tool to study time-series produced by all sorts of non-stationary dynamical systems. In this chapter, we first reviewed the main properties of DWT and the basic concepts related to the corresponding mathematical formalism. Next, we presented the way the DWT characterizes the type of dynamics embedded in the time-series. In general, the DWT reveals with high accuracy the dynamical features obeying power-like scaling properties of the processed signals and has been already successfully incorporated in the multifractal formalism. The interesting case of the time-series of the elementary cellular
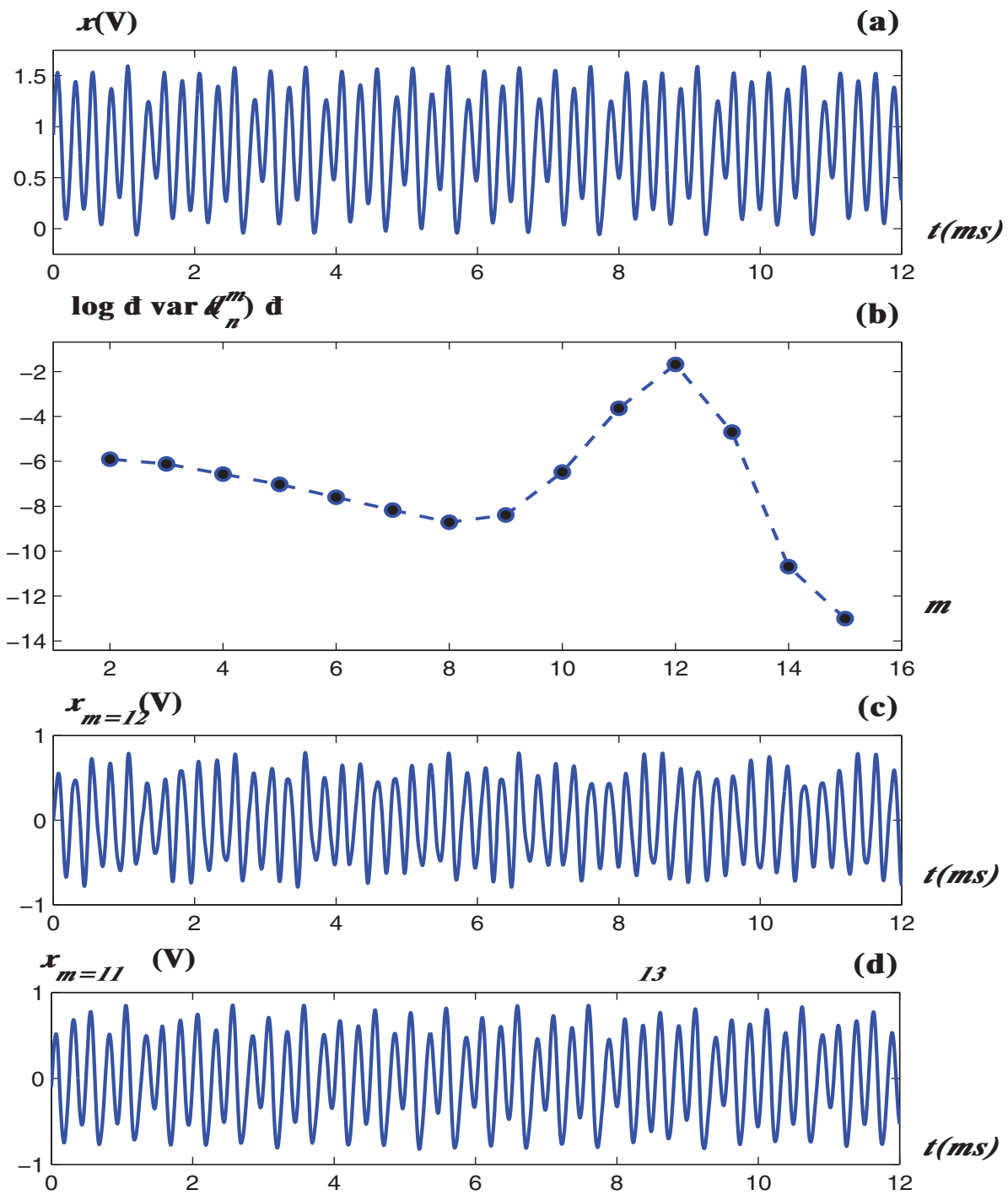
Fig. 8. The case $k = 0.4010$: (a) experimental time series of the x state, (b) wavelet coefficient variance, (c) time series of the 12th wavelet level, and (d) the time series of the sum from 11th to the 13th wavelet levels.
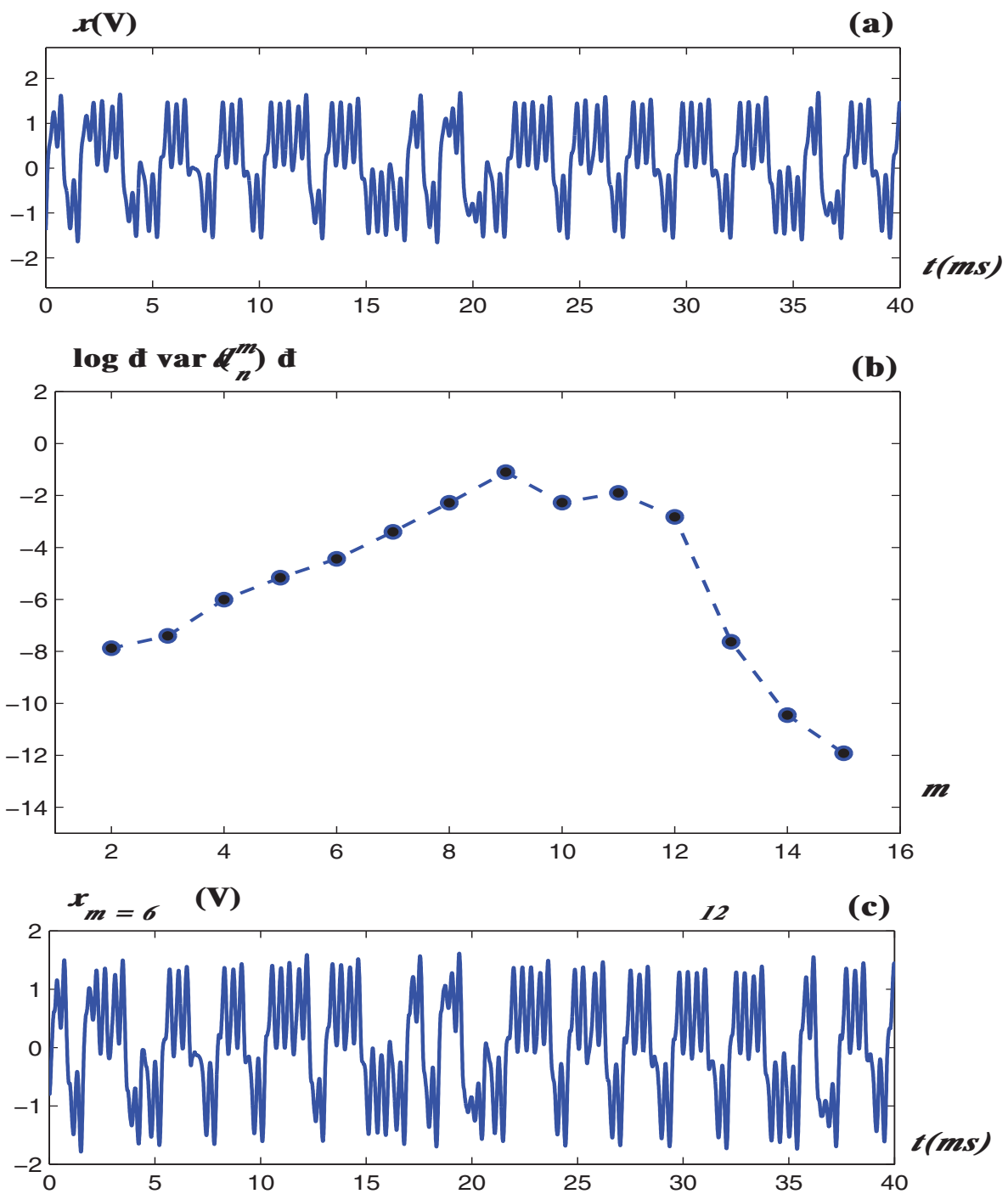
Fig. 9. The case $k = 0.3964$: (a) experimental time series of the x state, (b) wavelet coefficient variance, (c) time series of the sum from 6th to the 12th wavelet levels.

automata has been presented in the case of rule 90 and the concentration of energy by means of the concept of wavelet variance for the chaotic time-series of a three-state non-linear electronic circuit was also briefly discussed.

6. References

Campos-Cantón, E.; Murguía, J. S. & Rosu, H. C. (2008). Chaotic dynamics of a nonlinear electronic converter, *International Journal of Bifurcation and Chaos*, 18(10), October 2008 (2981-3000), ISSN 0218-1274.

Daubechies, I. (1992). *Ten lectures on Wavelets*, SIAM, ISBN 10: 0-89871-274-2, Philadelphia, PA.

Feder, J. (1998). *Fractals*, Plenum Press, ISBN 3-0642-851-2, New York, 1998 (Appendix B).

Halsey T.C.; Jensen M. H.; Kadanoff L. P.; Procaccia I. & Shraiman B. I. (1986). Fractal measures and their singularities: The characterization of strange sets, *Physical Review A*, 33(2), February 1986 (1141-1151), ISSN 1050-2947.

Kantelhardt, J.,W.; Zschinegner, S.,A.; Koscielny-Bunde, E.; Havlin, S.; Bunde, A. & Stanley. H. E. (2002). Multifractal detrended fluctuation analysis of nonstationary time series, *Physica A*, 316(1-4), December 2002 (87-114), ISSN 0378-4371.

Mallat, S. (1999).*A Wavelet Tour of Signal Processing*, 2nd. Edition, Academic Press, ISBN-13:978-0-12-466606-1, San Diego, California, USA.

Manimaran P.; Panigrahi P. K. & Parikh J. C. (2005). Wavelet analysis and scaling properties of time series, *Physical Review E*, 72(4) October 2005 (046120, 5 pages), ISSN 1539-3755.

Mejía M. & Urías J. (2001). An asymptotically perfect pseudorandom generator, *Discrete and Continuos Dynamical Systems*, 7(1), January 2001 (115-126), ISSN 1078-0947.

Murguía, J. S. & Campos-Cantón, E. (2006). Wavelet analysis of chaotic time series, *Revista Mexicana de Física*, 52(2), April 2006 (155-162), ISSN 0035-001X.

Murguía, J. S.; Pérez-Terrazas, J. E. & Rosu, H. C. (2009). Multifractal properties of elementary cellular automata in a discrete wavelet approach of MF-DFA, *Europhysics Letters*, 87(2), July 2009 (28003, 5 pages), ISSN 0295-5075.

Murguía, J. S.; Mejía-Carlos, M; Rosu, H. C. & Flores-Eraña, G. (2010). Improvement and analysis of a pseudo random bit generator by means of CA, *International Journal of Modern Physics C*, 21(6), June 2010 (741-756), ISSN 0129-1831.

Nagler J. & Claussen J. C. (2005). $1/f^\alpha$ spectra in elementary cellular automata and fractal signals, *Physical Review E*, 71(6) June 2005 (067103, 4 pages), ISSN 1539-3755.

Percival, D. B. & Walden, A. T. (2000) *Wavelet Methods for Time Series Analysis*, Cambridge University Press, ISBN 0-52164-068-7, Cambridge.

Rulkov, N. F. (1996). Images of synchronized chaos: Experiments with circuits, *CHAOS*, 6(3), September 1996 (262-279), ISSN 1054-1500.

Rulkov, N. F. & Sushchik, M. M.(1997). Robustness of Synchronized Chaotic Oscillations, *International Journal of Bifurcation and Chaos* 7(3), March 1997(625-643), ISSN 0218-1274.

Rulkov, N. F., Afraimovich, V. S., Lewis, C. T., Chazottes, J. R., & Cordonet, J. R. (2001). Multivalued mappings in generalized chaos synchronization. *Physical Review E* 64(1), July 2001(016217 1-11), ISSN 1539-3755.

Sanchez J. R. (2003). Multifractal characteristics of linear one-dimensional cellular automata, *International Journal of Modern Physics C*, 14(4), May 2003 (491-499), ISSN 0129-1831.

Staszewski, W. J. & Worden, K. (1999). Wavelet analysis of time series: Coherent structures, chaos and noise, *International Journal of Bifurcation and Chaos*, 9(3), September 1999 (455-471), ISSN 0218-1274.

Strang, G. & Nyugen, T. (1996). *Wavelets and Filter Banks*, Wellesley Cambridge Press, ISBN 0-96140-887-1, Wellesley, MA, USA.

Telesca L., Colangelo G., Lapenna V. & Macchiato M. (2004). Fluctuation dynamics in geoelectrical data: an investigation by using multifractal detrended fluctuation analysis, *Physics Letters A*, 332(5-6), November 2004 (398-404), ISSN 0375-9601.

Qian, S. (2002). *Introduction to Time-Frequency and Wavelet Transforms*, Prentice Hall PTR, ISBN 0-13030-360-7.

Wornell, G. W. & Oppenheim, A. V. (1992). Wavelet-based representations for a class of self-similar signals with application to fractal modulation, *IEEE Transactions on Information and Theory*, 38(2), 1992(785-800), ISSN 0018-9448.

Discrete Wavelet Transforms - Theory and Applications

Edited by Dr. Juuso T. Olkkonen

Discrete wavelet transform (DWT) algorithms have become standard tools for discrete-time signal and image processing in several areas in research and industry. As DWT provides both frequency and location information of the analyzed signal, it is constantly used to solve and treat more and more advanced problems. The present book: Discrete Wavelet Transforms: Theory and Applications describes the latest progress in DWT analysis in non-stationary signal processing, multi-scale image enhancement as well as in biomedical and industrial applications. Each book chapter is a separate entity providing examples both the theory and applications. The book comprises of tutorial and advanced material. It is intended to be a reference text for graduate students and researchers to obtain in-depth knowledge in specific applications.

How to reference

In order to correctly reference this scholarly work, feel free to copy and paste the following:

José S. Murguía and Haret C. Rosu (2011). Discrete Wavelet Analyses for Time Series, Discrete Wavelet Transforms - Theory and Applications, Dr. Juuso T. Olkkonen (Ed.), ISBN: 978-953-307-185-5, InTech, Available from: http://www.intechopen.com/books/discrete-wavelet-transforms-theory-and-applications/discrete-wavelet-analyses-for-time-series

INTECH
open science | open minds